

# Infrared Observation of Hot Cores <sup>\*</sup>

Bringfried Stecklum<sup>1</sup>, Bernhard Brandl<sup>2</sup>, Markus Feldt<sup>3</sup>, Thomas Henning<sup>4</sup>,  
Hendrik Linz<sup>1</sup>, and Ilaria Pascucci<sup>4</sup>

<sup>1</sup> Thüringer Landessternwarte Tautenburg, Sternwarte 5, D-07778 Tautenburg

<sup>2</sup> Center for Radiophysics & Space Research, Cornell University, Ithaca, NY 14853

<sup>3</sup> Max-Planck-Institut für Astronomie, Königstuhl 17, D-69117 Heidelberg

<sup>4</sup> Astrophysikalisches Institut und Universitäts-Sternwarte,  
Friedrich-Schiller-Universität Jena, Schillergäßchen 2-3, D-07745 Jena

**Abstract.** We report on mid-infrared imaging of hot cores performed with SpectroCam-10 and TIMMI2. The observations aimed at the detection of thermal emission presumably associated with the hot cores. Mid-infrared flux measurements are required to improve the luminosity and optical depth estimates for these sources. Results are presented for W3(H<sub>2</sub>O), G9.62+0.19, G10.47+0.03, and the possible hot core candidate G232.620+0.996. They illustrate that the morphology of these sources cannot be described by simple geometries. Therefore, line-of-sight effects and considerable extinction even at mid-infrared wavelengths must not be neglected.

## 1 Introduction

Hot cores (HCs) are the suspected birthplaces of high-mass stars ( $M \gtrsim 8 M_{\odot}$ ) [9]. Based on mm/submm interferometric results which provide sufficient angular resolution to separate HCs from neighbouring ultracompact HII regions (UCHIIs), first attempts were made to derive properties of the embedded high-mass stars as well as the surrounding envelope using infall models in combination with 1D radiative codes [11]. However, these results relied on the mm/submm part of the spectral energy distribution (SED) only. We performed infrared (IR) observations of HCs to provide flux densities (or at least upper limits) for the atmospheric 10 and 20  $\mu\text{m}$  spectral windows in order to complete the coverage of their SEDs with sub-arcsecond beam sizes and to investigate their morphology.

## 2 Observations and Data Reduction

The observations were carried out with SpectroCam-10 (SC 10) on the 5-m Hale<sup>1</sup> and TIMMI2 on the ESO 3.6-m telescopes. SC 10 is the Cornell-built 8–13  $\mu\text{m}$  spectrograph/camera [6] which utilizes a Rockwell 128×128 Si:As BIB array, providing a circular field of view (FOV) in imaging mode of 16'' (pixel size

<sup>\*</sup> Based on observations collected at the European Southern Observatory, La Silla, Chile, Proposal IDs 62.I-0530,67.C-0359

<sup>1</sup> Observations at the Palomar Observatory were made as part of a continuing collaborative agreement between the California Institute of Technology and Cornell University.

0'.25). The SC 10 imaging was performed in December 1998 and June 1999. The images were filtered using a wavelet algorithm [12] to enhance the signal-to-noise ratio (SNR). TIMMI2 is the new ESO thermal imaging multi-mode instrument covering the wavelength range from 5–20  $\mu\text{m}$  [14]. Its  $320 \times 240$  Si:As BIB array manufactured by Raytheon provides an unprecedented FOV in imaging mode of  $64'' \times 48''$  (pixel scale 0'.2) at 10 and 20  $\mu\text{m}$  and  $96'' \times 72''$  (pixel scale 0'.3) at 4.7  $\mu\text{m}$ . The observations were carried out in March 2001.

### 3 Results

#### 3.1 W3(H<sub>2</sub>O)/W3(OH)

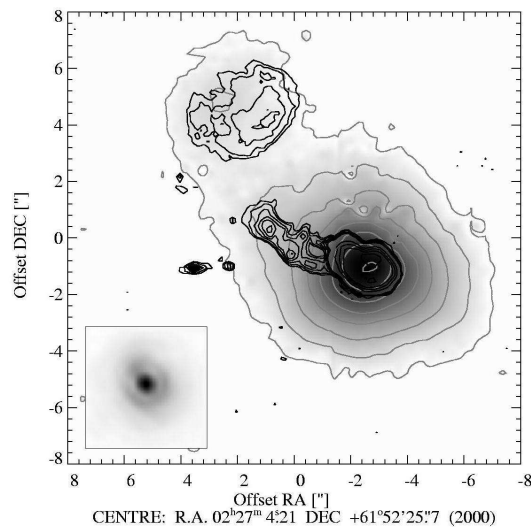


**Fig. 1.** SC 10 11.7  $\mu\text{m}$  image of W3(OH) with contours of the 11.7  $\mu\text{m}$  (grey) emission and of the 3.6 cm radio continuum (black, from [19]). W3(H<sub>2</sub>O) is located at the offset position [+3'.6,-1'.0]. The inset image of  $\alpha$  Tau indicates the beam size.

The HC W3(H<sub>2</sub>O) is located  $\sim 6''$  east of the UCHII W3(OH) at a distance of 2.2 kpc. The proper motion of its H<sub>2</sub>O masers [1] and the associated radio continuum jet [13] suggest recent outflow activity. Interferometric radio observations of W3(H<sub>2</sub>O) [21] yielded H<sub>2</sub> column densities of up to  $1.5 \times 10^{24} \text{ cm}^{-2}$  and rotation temperatures in the range of 160–200 K. The detection of the HC at mid-infrared (MIR) wavelengths was claimed by [8]. Fig. 1 shows the SC 10 image of W3(H<sub>2</sub>O)/W3(OH) with black contours delineating the 3.6 cm radio continuum [19]. W3(H<sub>2</sub>O) is at the offset position [+3'.6,-1'.0] and traced by its radio continuum jet, but is not detected at 11.7  $\mu\text{m}$ . The feature identified as W3(H<sub>2</sub>O) by [8] is presumably the weak cometary UCHII northeast of W3(OH). The radio position of the UCHII W3(OH) served as an astrometric reference.

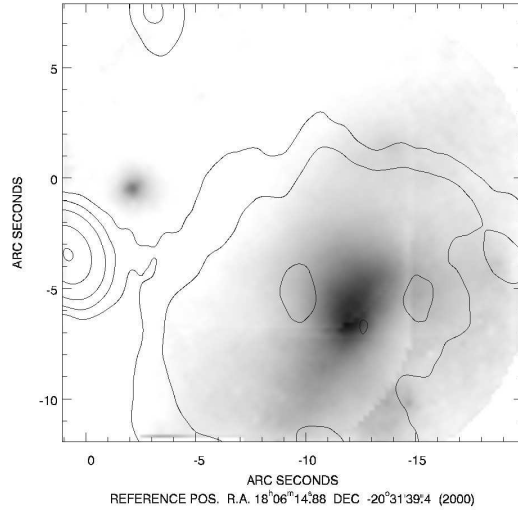


**Fig. 2.** SC 10  $11.7\mu\text{m}$  image of G9.62+0.19 with contours of the 1.3 cm radio continuum (from [3]).

The comparison of the spatial extent of W3(OH) with the standard star  $\alpha$  Tau (inset of Fig. 1) shows that it is clearly resolved.

The temperature and size derived from molecular line interferometry for W3(H<sub>2</sub>O) suggest that it should be a bright object in the MIR, with a predicted  $11.7\mu\text{m}$  flux density of  $\sim 2000$  Jy. Our failure to detect it despite a much better sensitivity ( $3\sigma$  point source detection limit of 6 mJy) than [8] implies a large amount of cold dust in front of the hot core. A detailed analysis of the SEDs of W3(H<sub>2</sub>O)/W3(OH) is given in [15].

### 3.2 G9.62+0.19

The object G9.62+0.19 (IRAS18032-2032) comprises several UCHIIIs at a distance of 5.7 kpc. Recently, weak radio continuum emission has been detected [17] at the location of the HC (component F) as well as outflow activity [7]. Remarkably, this object seems to be associated with  $2.2\mu\text{m}$  emission [16], a fact which can be hardly reconciled with spherical models of HCs. Such models imply extinction values which should prevent the detection of the HC at near-infrared (NIR) wavelengths. Fig. 2 shows the  $11.7\mu\text{m}$  SC 10 image of G9.62+0.19 with contours of the 1.3 cm radio continuum [3]. The bulk of the  $11.7\mu\text{m}$  emission stems from the extended radio component B which was used as astrometric reference. Surprisingly, no thermal emission was seen from the UCHII D which again implies a considerable optical depth even at MIR wavelengths for this source. This result concerning component D contradicts that of [5] due to differing astrometry. A pointlike source is obvious close to the location of the HC

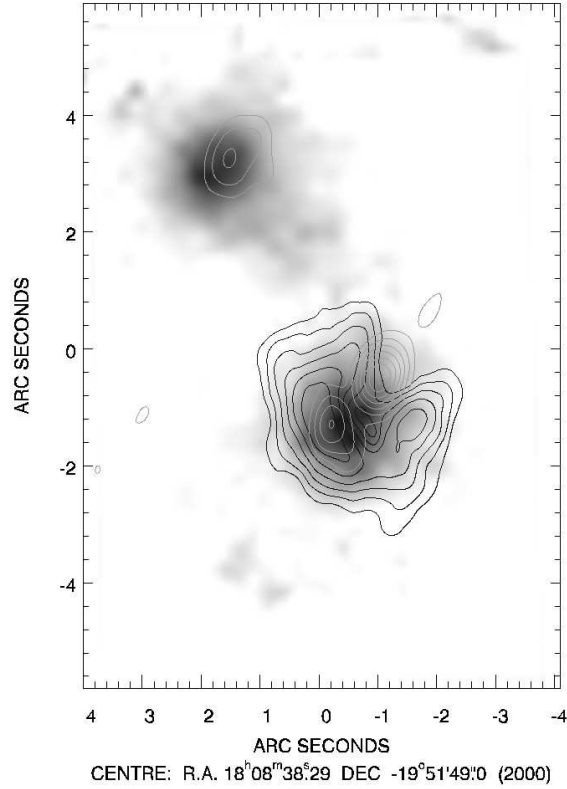


**Fig. 3.** SC 10 11.7  $\mu\text{m}$  image of G10.47+0.03 with contours of the 6 cm radio continuum (grey, from [20]) and of the  $\text{NH}_3(4, 4)$  line (black, from [4]).

(offset position  $[-2''.0, -1''.0]$ ). This emission is almost coincident with the 2.2  $\mu\text{m}$  feature. The poster contribution of Linz et al. (this volume) discusses this source and the relation of the observed IR emission to the recently detected molecular outflow [7] in more detail. Possibly, IR radiation arising from the HC escapes in the outflow lobe inclined towards the observer where the optical depth is lower.

### 3.3 G10.47+0.03

According to the radial brightness temperature profile based on interferometric maps of the  $\text{NH}_3(4,4)$  line, the HC G10.47+0.03 (IRAS18056-1952) seemed to be one of the rare cases with *established* evidence for internal heating by embedded OB stars contrary to external heating by adjacent UCHIIIs [4]. Two stars from the corresponding 2MASS images of the region were also detected with SC 10 at 11.7  $\mu\text{m}$ . They provide astrometric reference with sub-arcsecond precision. MIR emission from two sites in the G10.47+0.03 region was detected. These sources are not seen on the 2.2  $\mu\text{m}$  2MASS image ( $10\sigma$  detection limit of 1.2 mJy). Fig. 3 displays the SC 10 11.7  $\mu\text{m}$  image with contours of the 6 cm radio continuum

(grey, from [20]) and of the  $\text{NH}_3(4,4)$  emission (black, from [4]). The HC is located at the offset position  $[0''.0, -1''.6]$ . To the northwest of the HC, the  $\text{NH}_3$  emission is diminished due to absorption by the UCHII in the foreground. The centroid of the  $11.7\ \mu\text{m}$  radiation almost coincides with the center of the  $\text{NH}_3$  emission. A possible configuration which explains this morphology might be a cometary UCHII, similar to G29.96-0.02 and its adjacent HC (which are seen side-on), with the line of sight slightly inclined with respect to the symmetry axes of the HII region. The fact that there is only one MIR peak associated with the HC suggests that the multiple structure in the radio continuum (3 components are present in the map of [4]) is presumably due to locally enhanced plasma density and not caused by a few widely distributed high-mass stars. The lack of  $\text{NH}_3$  emission for the second MIR source (offset position  $[+1''.5, +3''.0]$ ) indicates that this is presumably a more evolved UCHII.

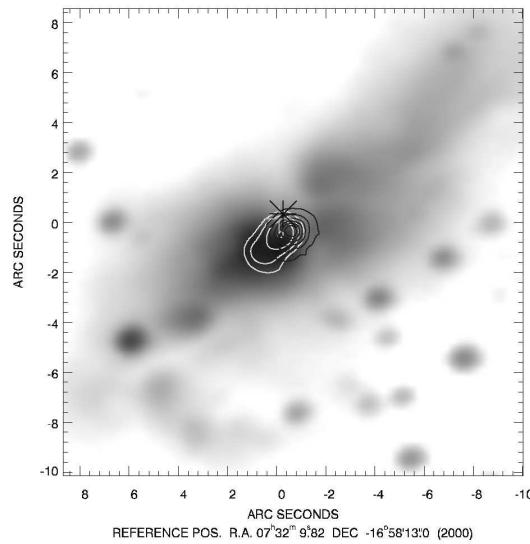


**Fig. 4.**  $2.2\ \mu\text{m}$  SOFI image of G232.620+0.996 with contours of the  $4.7\ \mu\text{m}$  (white) and the  $11.9\ \mu\text{m}$  (black) emission. The reference position is defined by the location of the masers. The black asterisk marks the location of the illuminating source derived from our  $2.2\ \mu\text{m}$  polarization map.

### 3.4 G232.620+0.996

The UCHII G232.620+0.996 (IRAS07299-1651) is associated with OH and  $\text{CH}_3\text{OH}$  masers [2],[18] which are signs of newly formed massive stars. The UCHII is  $1''.5$  northwest of the maser position [18]. These objects are located at the southern border of a dense core seen in the 1.3 mm map taken with the SEST [10]. Our  $2.2\ \mu\text{m}$  polarimetric map obtained with SOFI at the ESO-NTT revealed that the bipolar-like extended emission (see Fig. 4) at the southern rim of the dense

core is dominated by scattered light. The location of the illuminating source was derived by minimizing the sum of the scalar products between polarisation and radius vector as a function of source position. It is marked in Fig. 4 by the black asterisk, and situated very close to the masers and the UCHII. The large FOV of TIMMI2 covered the target and HD 60068 (situated  $47''$  northwest of it) simultaneously which allowed to establish accurate astrometry. A resolved IR source was found close to the maser position. Fig. 4 also displays contours of the  $4.7\ \mu\text{m}$  and  $11.9\ \mu\text{m}$  image taken with TIMMI2. It can be noticed that the emission peaks of both wavelengths are spatially offset, indicating a strong gradient in the optical depth in the immediate neighbourhood of the illuminating source.

## 4 Acknowledgements

This work was supported by DFG grants STE 605/17-1 and STE 605/18-1.

## References

1. J. Alcolea, K.M. Menten, J.M. Moran, M.J. Reid: In: *Astrophysical Masers*, ed. by A.W. Clegg & G.E. Nedoluha (Berlin: Springer), 225 (1993)
2. J.L. Caswell: MNRAS **297**, 215 (1998)
3. R. Cesaroni, E. Churchwell, P. Hofner, C.M. Walmsley: A&A **288**, 903 (1994)
4. R. Cesaroni, P. Hofner, C.M. Walmsley, E. Churchwell: A&A **331**, 709 (1998)
5. J.M. DeBuizer, R.K. Piña, C.M. Telesco: ApJS **130**, 437 (2000)
6. T.L. Hayward, J.W. Miles, J.R. Houck, G.E. Gull, J. Schoenwald J.: In: *Infrared Detectors and Instrumentation*, ed. by A.W. Fowler, Proc. SPIE, 1946, 334 (1993)
7. P. Hofner, H. Wiesemeyer, Th. Henning: ApJ **549**, 425 (2001)
8. E. Keto, D. Proctor, R. Ball, J. Arens, G. Jernigan: ApJ **401**, L113 (1992)
9. S. Kurtz, R. Cesaroni, E. Churchwell, P. Hofner, C.M. Walmsley: In: *Protostars and Planets IV*, ed. by V. Mannings, A.P. Boss, S.S. Russell, University of Arizona Press, Tucson, 299 (2000)
10. R. Klein, priv. comm. (2001)
11. M. Osorio, S. Lizano, P. D'Alessio: ApJ **525**, 808 (1999)
12. E. Pantin, J.-L. Starck: A&AS **118**, 575 (1996)
13. M.J. Reid, A.L. Argon, C.R. Masson, K.M. Menten, J.M. Moran: ApJ **443**, 238 (1995)
14. H.G. Reimann, H. Linz, R. Wagner, H. Relke, H.U. Käufel, E. Dietzsch, M. Sperl, J. Hron: In: *Optical and IR Telescope Instrumentation and Detectors*, ed. by M. Iye & A.F. Moorwood, Proc. SPIE **4008**, 1132 (2000)
15. B. Stecklum, B. Brandl, T.L. Hayward, Th. Henning, I. Pascucci, J. Wilson: A&A submitted, (2001)
16. L. Testi, M. Felli, P. Persi, M. Roth: A&A **329**, 233 (1998)
17. L. Testi, P. Hofner, S. Kurtz, M. Rupen: A&A **359**, L5 (2000)
18. A.J. Walsh, M.G. Burton, A.R. Hyland, G. Robinson: MNRAS **301**, 640 (1998)
19. D.J. Wilner D.J., W.J. Welch, J.R. Forster: ApJ **449**, L73 (1995)
20. D.O.S. Wood, E. Churchwell: ApJS **69**, 831 (1989)
21. F. Wyrowski, P. Schilke, C.M. Walmsley, K.M. Menten: ApJ **514**, L43 (1999)